European Spine Journal (2022) 31:1219–1227
https://doi.org/10.1007/s00586-022-07138-6

ORIGINAL ARTICLE

A sheep model of chronic cervical compressive myelopathy via an implantable wireless compression device

Zihe Li[1,2,3] · Shuheng Zhai[1,2,3] · Shanshan Liu[1,2,3] · Chunhua Chen[4] · Xinhu Guo[1,2,3] · Panpan Hu[1,2,3] · Ben Wang[1,2,3] · Youyu Zhang[1,2,3] · Feng Wei[1,2,3] · Zhongjun Liu[1,2,3]

Received: 7 April 2021 / Revised: 4 January 2022 / Accepted: 27 January 2022 / Published online: 22 February 2022

Abstract

Purpose This study aimed to establish an animal model in which we can precisely displace the spinal cord and therefore mimic the chronic spinal compression of cervical spondylotic myelopathy.

Methods In vivo intervertebral compression devices (IVCDs) connected with subcutaneous control modules (SCCMs) were implanted into the C2-3 intervertebral disk spaces of sheep and connected by Bluetooth to an in vitro control system. Sixteen sheep were divided into four groups: (Group A) control; (Group B) 10-week progressive compression, then held; (Group C) 20-week progressive compression, then held; and (Group D) 20-week progressive compression, then decompression. Electrophysiological analysis (latency and amplitude of the N1-P1-N2 wave in somatosensory evoked potentials, SEP), behavioral changes (Tarlov score), imaging test (encroachment ratio (ER) of intraspinal invasion determined by X-ray and CT scan), and histological examinations (hematoxylin and eosin, Nissl, and TUNEL staining) were performed to assess the efficacy of our model.

Results Tarlov scores gradually decreased as compression increased with time and partially recovered after decompression. The Pearson correlation coefficient between ER and time was $r = 0.993$ ($p < 0.001$) in Group B at 10 weeks and Groups C and D at 20 weeks. And ER was negatively correlated with the Tarlov score ($r = -0.878$, $p < 0.001$). As compression progressed, the SEP latency was significantly extended ($p < 0.001$), and the amplitude significantly decreased ($p < 0.001$), while they were both partially restored after decompression. The number of abnormal motor neurons and TUNEL-positive cells increased significantly ($p < 0.001$) with compression.

Conclusion Our implantable and wireless intervertebral compression model demonstrated outstanding controllability and reproducibility in simulating chronic cervical spinal cord compression in animals.

Keywords Cervical spondylotic myelopathy · Cervical spinal cord · Animal model · Implantable wireless compression device · Digital control

Background

Cervical spondylotic myelopathy (CSM) is one of the most common diseases causing spinal cord dysfunction. The most widely accepted mechanism underlying the pathogenesis of CSM is chronic spinal cord compression, which is related to intervertebral disk herniation, bone hyperplasia, ligament hypertrophy, ossification, and others [1, 2]. Current research on chronic spinal cord compression is mainly based on animal models and commonly used models, including screw placement compression3, water-absorbing material expansion [4–7], pressure balloon [8, 9], induced ossification compression [10], tumor compression [11], and magnetic resonance imaging (MRI)-guided focused ultrasound

Zihe Li and Shuheng Zhai have contributed to the work equally and should be regarded as co-first authors.

Three of all authors Zihe Li, Feng Wei and Zhongjun Liu have patents CN201310033774.X and CN201320047762.8 both licensed to Peking University Third Hospital.

A sheep model of chronic cervical compressive myelopathy via an implantable wireless compression device.

✉ Feng Wei
weifeng@bjmu.edu.cn

Extended author information available on the last page of the article

compression models [12]. However, all these models have common drawbacks, such as poor controllability, high risk of surgical trauma and infection, and poor reproducibility. In a study conducted by Kim et al. [6], polyurethane material, which could absorb water and expand, was placed into the spinal canal to achieve chronic compression of the spinal cord. However, accuracy of the compression was difficult to evaluate. Karadimas et al. [10] simulated the pathogenesis of cervical spinal cord compression, caused by the ossification of the ligamentum flavum, by promoting local calcium and phosphorus deposition and new bone formation. However, the compression caused by the ossification-inducing material was not controllable, and the process of inducing ossification between different experimental animals lacked consistency and repeatability. Controllable compression is the key to reliable animal models, the lack of which limits further in-depth studies. Advances in materials science, optoelectronic devices, system engineering, and mechanics design have offered compelling options [13, 14]. The appearance of miniaturized, fully implantable platforms with wireless capabilities and battery-free operation makes biocompatibility and controllability possible.

In this study, an in vitro control system using wireless Bluetooth technology to regulate the in vivo intervertebral compression device (IVCD) was used to achieve controllable compression in an animal model of chronic cervical spinal cord compression, which can remotely control the IVCD to reduce trauma and control the compression precisely. Sheep were used to establish the animal model in this study due to the good similarity between the anatomical and biomechanical characteristics of the sheep spine and the human spine [15, 16].

Methods

Compression device

The spinal cord mechanical compression device comprised two parts: an in vivo IVCD and subcutaneous control module (SCCM) (Fig. 1; the size of the IVCD outer component was 8 × 11.3 × 24 mm and made of polyether ether ketone). The IVCD was equipped with a miniature reducer motor, metal push rod with a rubber head, transmitter lead, and spring. The head of the metal push rod was threaded, and a nylon compression head was screwed. The reducer motor was connected to the drive lead, which could maximally extend the push rod in the slide to 13 mm. The extrusion head radius was an umbrella with a radius of 2 mm and a thickness of 1.5 mm. The operating accuracy was 0.1 mm. The system self-locks when the motor stops. When the motor is reversed, the spring retracts the pushrod. The SCCM is composed of a control chip, Bluetooth module, and lithium battery controlled by a magnetic switch. The in vivo SCCM was fixed under the skin of sheep's neck. The IVCD and in vivo SCCM were connected by a wire to receive the signal of the in vitro control system. The entire compression device was sealed with a silicon film with good biocompatibility. A stainless steel plate (316 L) with screws was used to fix the IVCD into the C2-3 intervertebral disk space.

The in vitro system was controlled by built-in software named EASYPUSH v1.05 in an Android mobile phone and connected with Bluetooth, which was a transmission software based on RFCOMM Bluetooth serial port service. Through this software, it could connect Bluetooth serial port module for communication and realize serial port connection

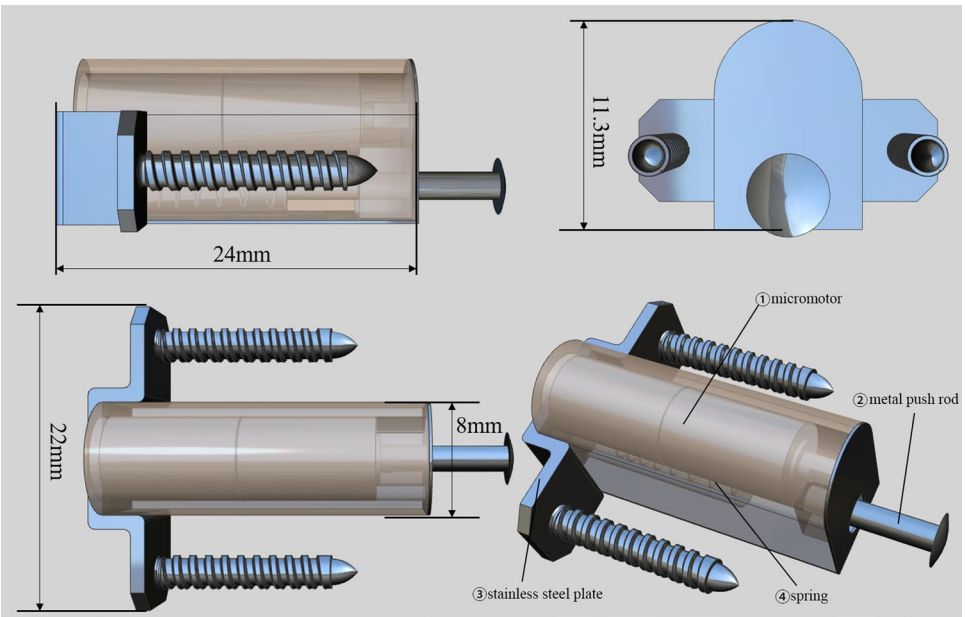

Fig. 1 The in vivo intervertebral compression device (IVCD) was equipped with ① a micromotor, ② a metal push rod with a rubber head, ③ a stainless steel plate, and ④ a spring. The push rod could be extended or retracted by the reducer motor

of mobile phones and send a set of control instructions defined by itself to the microcontroller (Author: Lisn3188. Platform: android2.2 and above). Pushing distances were controlled by the number of input current pulses. The device has been calibrated before implantation so that we could determine the availability of our device and the motor turned nearly the same number of turns under each pulse.

Experimental animals

Sixteen adult male small-tailed Han sheep weighing 45 kg on average were randomly divided into four groups, with four animals in each group: Group A (control), Group B (10 weeks of compression), Group C (20 weeks of compression), and Group D (decompression after 20 weeks of compression). After the operation, compression was not applied in Group A. In Groups B, C, and D compression displacement of 0.1 mm was added every 2 days. In Group B, the compression was stopped at the end of week 10 and the sheep were observed for another 10 weeks, and euthanasia was performed at the end of week 20. In Group C, the oppression was stopped at the end of the 20th week, and euthanasia was performed at the end of the 30th week after 10 weeks of observation. In Group D, the pushrod was stopped and completely withdrawn at 20 weeks and the sheep were euthanized at the end of week 30 after 10 weeks of observation. The sheep were euthanized with pentobarbital sodium overdose. This study was approved by the Experimental Animal Welfare Ethics Branch of the Peking University Biomedical Ethics Committee (Ethics prove: A2020391).

Surgical placement of compression devices

After intravenous anesthesia, the sheep were placed in the supine position, and a right longitudinal incision was made through the anterior cervical approach to the front of the cervical vertebral body. Intraoperative radiographs confirmed the C2-3 intervertebral space. The intervertebral disk was removed to the posterior edge of the vertebral body. A curette and grinding drill were used to expand the space to the size of the compression device, and the compression device was fixed at the C2-3 intervertebral space with plates and screws. The initial position of the head of the pushrod was at the posterior edge of the vertebral body (Fig. 2), and SCCMs were implanted under the skin.

Intraoperative and postoperative electrophysiological examination

Electrophysiological examinations were performed immediately after the operations at 1, 10, 20, and 30 weeks postoperatively. The somatosensory evoked potential (SEP) was assessed after anesthesia. A NicoletVikingIV (Nicolet Biomedical, USA) electrophysiology instrument and an electrode (13R25, Dantec, Denmark) were used for stimulation and recording; the earth pole was at the right forelimb, and the stimulation site was in proximity to the median nerve of the left forelimb. The stimulation intensity was 50–60 V, the frequency was 3.7 Hz, and a duration was 0.2 ms. The recording electrodes were located in the midline of the forehead. The stacking fold was 512. The latency and amplitude of the N1-P1-N2 wave were determined. Records were obtained three times, and the average values were calculated.

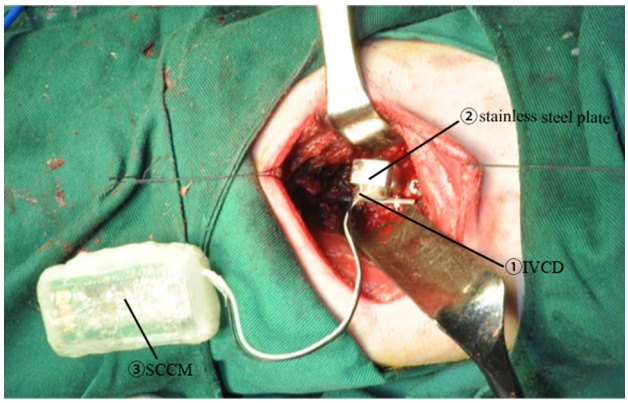

Fig. 2 The in vivo subcutaneous control module was fixed at the defect of the intervertebral space. ① In vivo intervertebral compression device (IVCD); ② stainless steel plate; and ③ subcutaneous control module (SCCM)

Behavioral observation and imaging examination

Behavioral analyses were performed before and immediately after the operation and at 1, 5, 10, 20, and 30 weeks after the operation. The Tarlov scores for each sheep in the group were obtained by three observers who were blinded to the group designations and then averaged for the groups [3, 17]. Cervical X-ray and computed tomography (CT) examinations were performed before and immediately after surgery.

Cervical CT scans were also performed at 1, 5, 10, 15, 20, and 30 weeks after the operation, and the encroachment ratio (ER) of intraspinal invasion was calculated (Fig. 3). Encroachment ratio was defined by ER = (1-MD/CD)100%, where MD is the minimal distance between the screw and the posterior canal wall and CD is canal diameter, both at the level of compression.

Histological examination

Spinal cord tissue samples were taken at 20 weeks in Group B and at 30 weeks in Groups A, C, and D. A 4% paraformaldehyde perfusion fixative solution was used for cardiac perfusion. For histological observation, the spinal cord (8 mm from rostral to caudal) from the compression

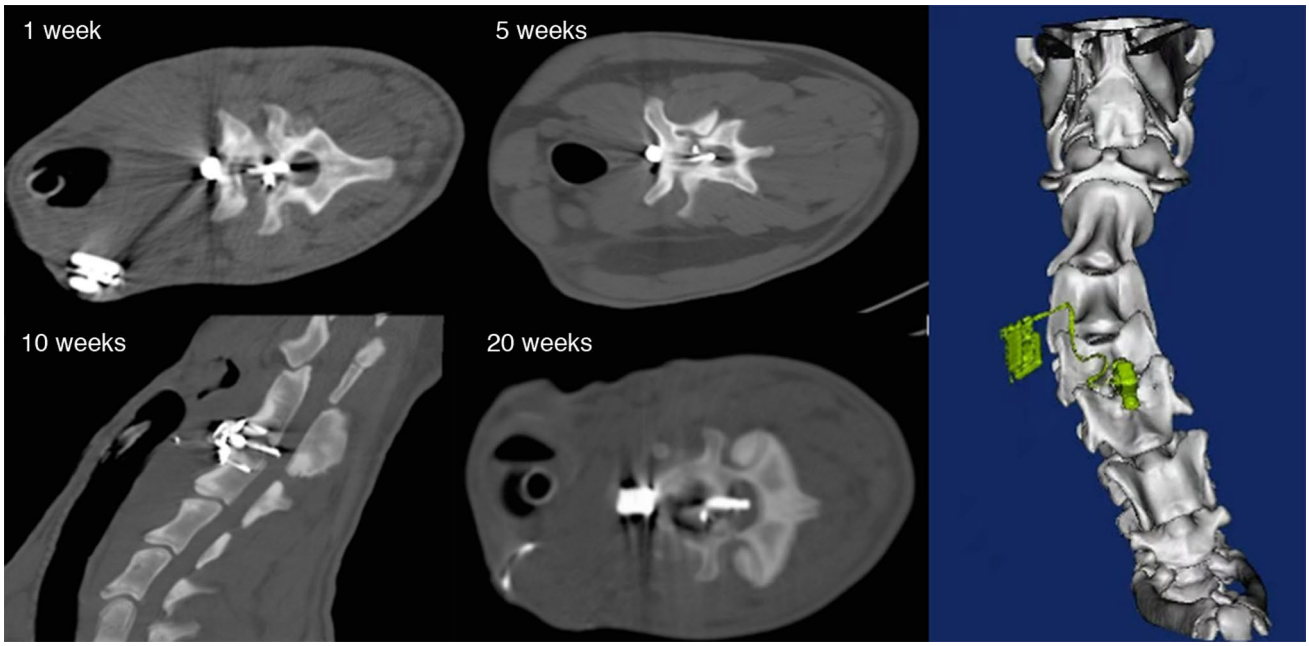

Fig. 3 Cervical CT scans of one sheep in Group D at 1, 5, 10, and 20 weeks after the operation. The spinal canal encroachment ratio increased with the extension of the pushrod. The in vivo subcutaneous control module and integrated circuits are shown in 3D CT reconstruction

center of the C2-3 spinal cord segment was dissected out, fixed with 4% PFA overnight, and cut into coronal sections of 10 μm thickness. Hematoxylin and eosin (HE) staining and Nissl staining were performed to observe the morphological changes of cells in the anterior horn and the corticospinal tract in the white matter of the spinal cord. Apoptosis of corticospinal tract nerve fibers was assessed by TUNEL (terminal deoxynucleotidyl transferase dUTP nick end labeling) staining. We observed the TUNEL staining slices under high view of microscope (200×) and randomly selected five visual field to count the positive fluorescent staining cells and analyzed the difference among groups.

Statistical methods

Data were analyzed with SPSS20.0. Tarlov scores were compared between groups using the rank-sum test. The Pearson correlation coefficient and general linear regression were used to evaluate the association between ER and time. The relationship between ER and Tarlov score was assessed using the Pearson correlation coefficient. Unpaired t tests following with post hoc correction were used to compare the SEP results, proportion of cells with histologically abnormal morphology, and number of positive cells detected by TUNEL staining. $P < 0.05$ was considered statistically significant.

Results

None of the animals died during the operation. Complications such as infection, dysphagia, leakage of the esophagus and trachea, or loosening of the device were not observed after operations. One sheep in Group B had the SCCM break down 24 days after the operation, which was corrected by replacing the SCCM in a second operation on Day 26.

Imaging observation

The ER in Group B was 33.0 ± 1.8% at 10 weeks and 64.8 ± 1.9% and 66.3 ± 3.2% in Groups C and D, respectively, at 20 weeks (Table 1). The Pearson correlation coefficient between ER and time in Groups B, C, and D

Table 1 Encroachment ratio of Groups B, C, and D (Mean ± SD, $n = 4$, %)

Time	Group B	Group C	Group D
1 week	2.8 ± 0.4	2.4 ± 0.6	2.5 ± 0.7
5 weeks	15.8 ± 0.9	15.6 ± 0.8	15.2 ± 1.0
10 weeks	33.0 ± 1.8	31.2 ± 1.3	31.1 ± 1.3
15 weeks	/	46.9 ± 1.4	45.8 ± 1.6
20 weeks	32.8 ± 0.6	64.8 ± 1.9	66.3 ± 3.2
30 weeks	/	61.5 ± 2.7	1.25 ± 1.3

SD Standard deviation

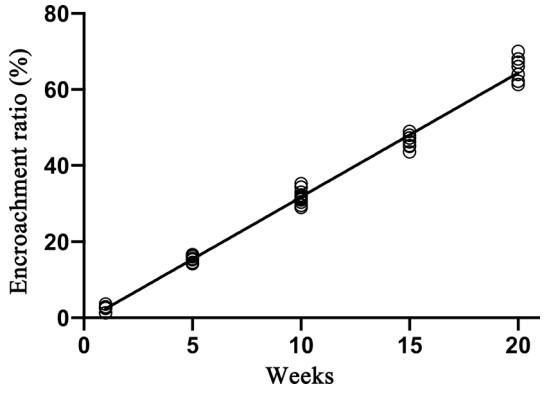

Fig. 4 The spinal canal encroachment ratio in each group at 1, 5, 10, 15, and 20 weeks after the operation during the pushing period. The slope of this linear fitting equation is 3.26%/week. R2 = 0.993

Table 2 Tarlov score of Groups A, B, C, and D after surgery (Mean ± SD, $n = 4$)

Time	Group A	Group B	Group C	Group D
1 week	5.0 ± 0.0	5.0 ± 0.0	5.0 ± 0.0	5.0 ± 0.0
5 weeks	5.0 ± 0.0	4.8 ± 0.4	5.0 ± 0.0	5.0 ± 0.0
10 weeks	5.0 ± 0.0	4.5 ± 0.5	4.3 ± 0.4	4.5 ± 0.5
15 weeks	5.0 ± 0.0	/	3.5 ± 0.5	3.8 ± 0.4
20 weeks	5.0 ± 0.0	4.5 ± 0.5	2.8 ± 0.4	2.5 ± 0.5
30 weeks	5.0 ± 0.0	/	2.5 ± 0.5	3.8 ± 0.4

Tarlov score: 0—no voluntary activity of any kind; 1—muscle contraction could be observed after the needle was inserted in the body; 2—joint movement was visible, though the patient could not bear weight; 3—the patient was able to bear weight but could not jump; 4—the patient was able to jump but limped; and 5 points, normal jumping posture. *SD*: Standard deviation

was $r = 0.993$ ($p < 0.001$); the linear regression equation between ER and time (t) during the pushing period was ER (%) = 3.26 × t (Fig. 4). ER was negatively correlated with the Tarlov score (Pearson correlation coefficient $r = -0.878$, $p < 0.001$). However, the data in Group D at 30 weeks did not follow the correlation, with low ER and Tarlov scores.

Behavioral observation

Average Tarlov scores for each group reported as a function of time are reported in Table 2. Functional behavior deficits were assessed in all animals within 1 to 2 days after the operation. Tarlov scores were 5 in all the animals in Group A throughout our observation period. In Group B, two scored 5, and two scored 4 at the end of 10 weeks and did not change by the end of 20 weeks. In Group C, three scored 3 and one scored 2 at the end of 20 weeks and, similarly to Group B, did not change by the end of 30 weeks. In Group D, two scored 3 and two scored 2 at 20 weeks, while unlike Groups B and C, Group D improved with three scored 4 and one scored 3 by the end of 30 weeks. The behavioral scores in Group C were not significantly different from those in Group D at 20 weeks but were significantly different from those of Groups A and D at the end of 30 weeks ($P < 0.001$, Table 2).

Electrophysiological monitoring

During and immediately after the operation, the latency and amplitude did not change significantly in any animal. The SEP latency and amplitude of the animals in Groups B, C, and D were not significantly different from those in group A immediately or 1 week after the operation. However, at 10 and 20 weeks, the latency in Groups B, C, and D was significantly prolonged ($p < 0.001$), and the amplitude was significantly lower than that in Group A ($p < 0.001$). At 30 weeks, the latency in Group D was significantly shorter than that in Group C ($p < 0.001$), while the amplitude was significantly higher than that in Group C ($p < 0.001$) (Table 3).

Histological examination

All spinal cord tissue sections were in good shape. HE staining showed normal anterior horn motor neurons and corticospinal tract nerve fibers in sections of Group A (Fig. 5A1, A3). Atrophy of motor neurons of the anterior horn was observed in sections of Group B (Fig. 5B1, B3), with a reduced number of neurons and wide space around the

Table 3 Latency and amplitude of SEP

Postoperative	Latency (ms)				Amplitude (μV)			
	Group A	Group B	Group C	Group D	Group A	Group B	Group C	Group D
Immediately	12.33 ± 1.63	13.01 ± 1.55	12.09 ± 1.73	11.67 ± 1.26	2.80 ± 0.41	2.88 ± 0.59	2.89 ± 0.58	3.08 ± 0.33
1 week	12.55 ± 1.65	14.88 ± 1.38	15.24 ± 1.05	13.00 ± 1.13	2.71 ± 0.43	2.13 ± 0.35	2.19 ± 0.34	2.37 ± 0.37
10 weeks	/	20.14 ± 1.03	19.04 ± 1.30	18.18 ± 0.81	/	1.40 ± 0.24	1.33 ± 0.19	1.46 ± 0.15
20 weeks	12.15 ± 1.62	20.43 ± 0.73	23.78 ± .271	23.80 ± 1.44	2.67 ± 0.53	1.44 ± 0.21	0.99 ± 0.22	0.89 ± 0.18
30 weeks	/	/	23.45 ± 2.29	19.53 ± 1.21	/	/	0.89 ± 0.10	1.41 ± 0.22

SEP Somatosensory evoked potential

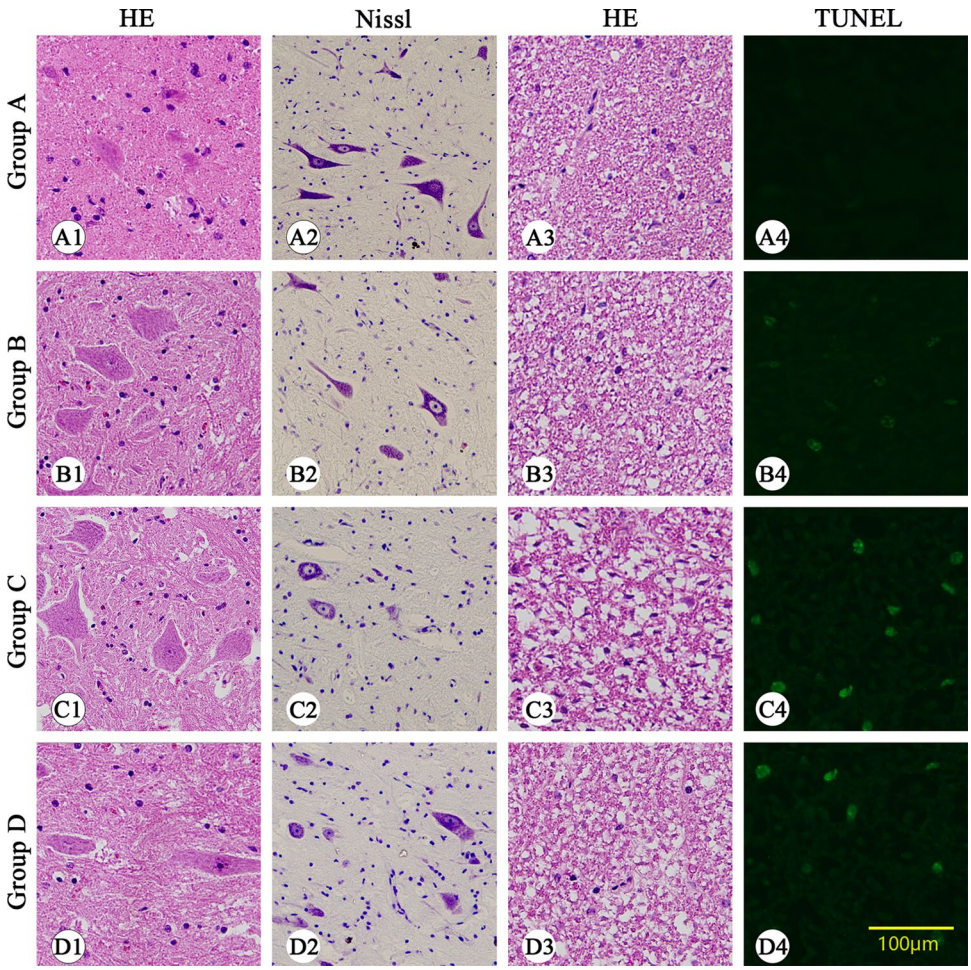

Fig. 5 Hematoxylin and eosin staining and Nissl and TUNEL staining were performed on the tissue sections of all groups. Normal motor neurons within anterior horn were observed in sections of Group A. Meanwhile, varying degrees of abnormalities were observed in Groups B, C, and D. TUNEL-positive cells were not observed in Group A. However, positive cells appeared in Groups B, C, and D

neurons. We also observed a reduced number of Nissl bodies in Group B compared to Group A (Fig. 5B2). Demyelination of the corticospinal tract axon and vacuolar degeneration appeared in Group B (Fig. 5B3). These findings were more obvious in Groups C and D, wherein the motor neuron cell body became flat in the extrusion direction. TUNEL staining (Fig. 5A4-D4) showed that the number of fluorescence-positive cells increased significantly with compression. There were significant differences in the proportion of abnormal motor neuron cells shown in Fig. 5A3, B3, C3, and D3. The number of TUNEL-positive cells increased significantly after compression, as shown in Fig. 5A4, B4, C4, and D4 ($p < 0.01$). However, no significant difference was observed between Group D and Group C in HE and TUNEL staining (Figs. 6 and 7).

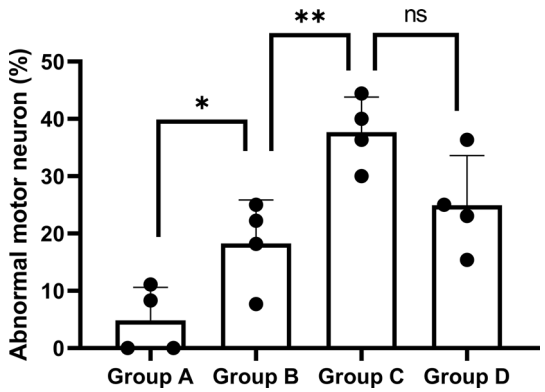

Fig. 6 Statistical analysis of the percentage of abnormal motor neurons observed from the HE staining results. * $p < 0.05$; ** $p < 0.01$; and ns: no significant difference

Discussion

ER has often been used to describe the degree of spinal stenosis or spinal cord compression [9, 18]. In our study, the behavioral scores of all groups were maintained after 1 week of operation. While Group A did not show any change in behavioral scores with time, as the degree of compression gradually increased in Groups B, C, and D, the behavioral scores gradually declined. Groups C and D showed obvious manifestations of neurological impairments by the end of

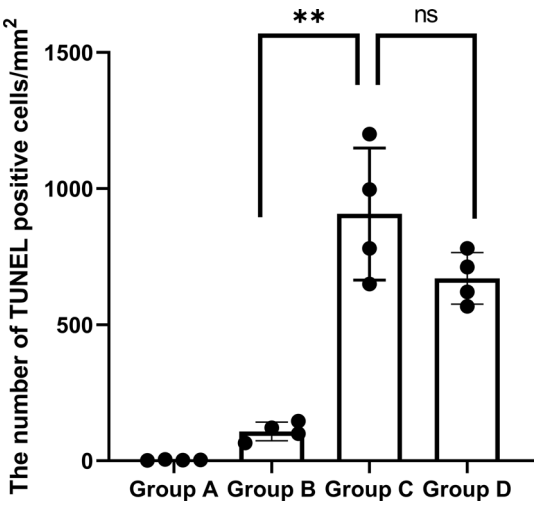

Fig. 7 Statistical analysis of the results of TUNEL staining. The number of TUNEL-positive cells was counted within five randomly selected visual field under high-power field of microscope (200×). ** $p < 0.01$; ns: no significant difference

the experiment with some recovery noted in Group D after decompression. This suggests that enough compression can effectively damage nerve function, and decompression can partially improve nerve function.

We found that spinal canal ER was negatively correlated with the degree of neurological damage (r = -0.862, p< 0.001). An imaging study demonstrated that the spinal canal ER of Groups B, C, and D gradually increased with time, showing a good linear relationship with time t (r =0.998), suggesting that the degree of compression can be controlled by the number of electrical pulses or the duration of the stimulation in our model. Therefore, we reduced the number of imaging observations and amount of anesthetics being administered [19, 20] and reduced the cost of the experiment and the possible impact of multiple operations on animals.

SEP has been used for the diagnosis of CSM and recovery evaluation and is commonly used in animal models. Animals with spinal cord injury usually show amplitude reduction and prolonged latency [9, 21]. In our study, as the degree of compression progressed, the latency was significantly extended, and the amplitude decreased. When compression was completely relieved, the latency was significantly decreased, and the amplitude increased, although it did not return to a normal value. One limitation of this device is that, due to the limited number of measurement time points, the association needs to be further studied.

In the histological study, we noticed that in Group B, as compression progressed, neuron atrophy occurred and the number of neurons decreased, while the space around neurons widened, and the nerve fiber showed mild demyelination and vacuolar degeneration. In Groups C and D, the neuron cell bodies showed obvious degenerative atrophy, the Nissl bodies were reduced, nerve fibers showed extensive demyelination and degeneration, and the cell bodies flattened in the extrusion direction. At the same time, the number of TUNEL-positive cells increased with the progression of compression, suggesting that the number of apoptotic cells might be positively correlated with the degree of compression, which is consistent with many previous studies [3, 12, 22], suggesting the reliability of this model to mimic the pathogenesis of CSM. We were not able to observe significant improvement in histology after completely relieving the compression. Further investigations are needed to explore the association between histological changes and the time and degree of compression.

While the Tarlov scores decreased, the SEP latency increased and SEP amplitude decreased in the time when encroachment was increased (Group B 0–10 weeks and Group C 0–20 weeks), in the period when the encroachment was held constant (Group B: 10–20 weeks and Group C: 20–30 weeks) Tarlov scores, SEP latency, and amplitude remained without significant change. This suggests that the immediate response to mechanical compression was directly responsible for the observed changes and not delayed consequences from mechanical compression.

However, MRI examination would be difficult once the micromotor device is inserted into the intervertebral space, which may limit the device's application in imaging research. In the future, we can better simulate the occurrence and treatment of different types of cervical spondylosis by modifying the compression procedure.

In conclusion, our study set up a novel, digital remote-controlled animal model to simulate chronic cervical spinal cord compression, with good controllability and high repeatability, without secondary surgery. Moreover, the materials of our compression device are easily accessible and low in cost, facilitating wide application of the device. Our study is the first to apply implantable and wireless devices in animal CSM models, achieving gratifying results, and providing new ideas for the implantation of wireless devices into animal models and even clinics.

Authors' contributions All authors contributed to the study conception and design. Material preparation, data collection, and analysis were performed by Shuheng Zhai, Shanshan Liu, Xinhu Guo, Ben Wang, and Youyu Zhang. Animal experiments were completed by Zihe Li, Chunhua Chen, and Panpan Hu. The first draft of the manuscript was written by Zihe Li, Shuheng Zhai, and Shanshan Liu. Feng Wei and Zhongjun Liu revised the manuscript.

Funding This study was supported by grants from Peking university biomedical engineering interdisciplinary research fund.

Availability of data and material Yes.

Code availability Yes.

Declarations

Conflict of interest All authors declare that they have no conflict of interest.

Ethics approval This study was approved by the Ethics Committee of Peking University Third Hospital (NO. A2020391).

References

1. Cao P, Zheng Y, Zheng T, Sun C, Lu J, Rickett T, Shi R (2014) A model of acute compressive spinal cord injury with a minimally invasive balloon in goats. J Neurol Sci 337:97–103
2. Gutruf P, Rogers JA (2018) Implantable, wireless device platforms for neuroscience research. Curr Opin Neurobiol 50:42–49
3. Hu Y, Wen CY, Li TH, Cheung MM, Wu EX, Luk KD (2011) Somatosensory-evoked potentials as an indicator for the extent of ultrastructural damage of the spinal cord after chronic compressive injuries in a rat model. Clin Neurophysiol 122:1440–1447
4. Ijima Y, Furuya T, Koda M, Matsuura Y, Saito J, Kitamura M, Miyamoto T, Orita S, Inage K, Suzuki T, Yamazaki M, Ohtori S (2017) Experimental rat model for cervical compressive myelopathy. NeuroReport 28:1239–1245
5. Jiang H, Wang J, Xu B, Yang H, Zhu Q (2017) A model of acute central cervical spinal cord injury syndrome combined with chronic injury in goats. Eur Spine J 26:56–63
6. Karadimas SK, Gatzounis G, Fehlings MG (2015) Pathobiology of cervical spondylotic myelopathy. Eur Spine J 24(Suppl 2):132–138
7. Karadimas SK, Moon ES, Yu WR, Satkunendrarajah K, Kallitsis JK, Gatzounis G, Fehlings MG (2013) A novel experimental model of cervical spondylotic myelopathy (CSM) to facilitate translational research. Neurobiol Dis 54:43–58
8. Kim P, Haisa T, Kawamoto T, Kirino T, Wakai S (2004) Delayed myelopathy induced by chronic compression in the rat spinal cord. Ann Neurol 55:503–511
9. Kubota M, Kobayashi S, Nonoyama T, Shimada S, Takeno K, Miyazaki T, Guerrero AR, Iwamoto H, Baba H (2011) Development of a chronic cervical cord compression model in rat: changes in the neurological behaviors and radiological and pathological findings. J Neurotrauma 28:459–467
10. Malka R, Guarin DL, Mohan S, Hernandez IC, Gorelik P, Mazor O, Hadlock T, Jowett N (2020) Implantable wireless device for study of entrapment neuropathy. J Neurosci Methods 329:108461
11. Manabe S, Tanaka H, Higo Y, Park P, Ohno T, Tateishi A (1989) Experimental analysis of the spinal cord compressed by spinal metastasis. Spine (Phila Pa 1976) 14:1308–1315
12. Morishita Y, Hida S, Naito M, Matsushima U (2005) Evaluation of cervical spondylotic myelopathy using somatosensory-evoked potentials. Int Orthop 29:343–346
13. Morris SH, Howard JJ, El-Hawary R (2017) Comparison of motor-evoked potentials versus somatosensory-evoked potentials as early indicators of neural compromise in rat model of spinal cord compression. Spine (Phila Pa 1976) 42:E326–E331
14. Nardone R, Holler Y, Brigo F, Frey VN, Lochner P, Leis S, Golaszewski S, Trinka E (2016) The contribution of neurophysiology in the diagnosis and management of cervical spondylotic myelopathy: a review. Spinal Cord 54:756–766
15. Wilke HJ, Kettler A, Claes LE. Are sheep spines a valid biomechanical model for human spines? Spine (Phila Pa 1976). 1997 15;22(20):2365–74.
16. Wilke HJ, Kettler A, Wenger KH (1997) Anatomy of the sheep spine and its comparison to the human spine. Anat Rec 247(4):542–555
17. Oakden W, Kwiecien JM, O'Reilly MA, Lake EM, Akens MK, Aubert I, Whyne C, Finkelstein J, Hynynen K, Stanisz GJ (2014) A non-surgical model of cervical spinal cord injury induced with focused ultrasound and microbubbles. J Neurosci Methods 235:92–100
18. Tetreault L, Goldstein CL, Arnold P, Harrop J, Hilibrand A, Nouri A, Fehlings MG (2015) Degenerative cervical myelopathy: a spectrum of related disorders affecting the aging spine. Neurosurgery 77(Suppl 4):S51-67
19. Wang L, Wang Y, Shi L, Liu P, Kang J, He J, Liu Y, Li D (2019) Can the sheep model fully represent the human model for the functional evaluation of cervical interbody fusion cages? Biomech Model Mechanobiol 18:607–616
20. Yamamoto S, Kurokawa R, Kim P (2014) Cilostazol, a selective Type III phosphodiesterase inhibitor: prevention of cervical myelopathy in a rat chronic compression model. J Neurosurg Spine 20:93–101
21 Yoshizumi T, Murata H, Yamamoto S, Kurokawa R, Kim P, Kawahara N (2016) Granulocyte Colony-Stimulating Factor Improves Motor Function in Rats Developing Compression Myelopathy. Spine (Phila Pa 1976) 41:E1380–E1387
22. Zhou SY, Yuan B, Qian C, Chen XS, Jia LS (2018) Evaluation of measuring methods of spinal canal occupation rate in thoracic ossification of ligamentum flavum. World Neurosurg 110:e1025–e1030

Authors and Affiliations

Zihe Li[1,2,3] · Shuheng Zhai[1,2,3] · Shanshan Liu[1,2,3] · Chunhua Chen[4] · Xinhu Guo[1,2,3] · Panpan Hu[1,2,3] · Ben Wang[1,2,3] · Youyu Zhang[1,2,3] · Feng Wei[1,2,3] · Zhongjun Liu[1,2,3]

Zihe Li
skyhealth@qq.com

Shuheng Zhai
sykkjgxs@163.com

Shanshan Liu
1039165305@qq.com

Chunhua Chen
cch@bjmu.edu.cn

Xinhu Guo
guoxinhu007@foxmail.com

Panpan Hu
pphu@bjmu.edu.cn

Ben Wang
clumsypku@163.com

Youyu Zhang
287572497@qq.com

Zhongjun Liu
zjliu@bjmu.edu.cn

[1] Department of Orthopaedics, Peking University Third Hospital, 49 North Garden Road, Haidian District, Beijing 100191, China

[2] Engineering Research Center of Bone and Joint Precision Medicine, Ministry of Education, Beijing, China

[3] Beijing Key Laboratory of Spinal Disease Research, Beijing, China

[4] Department of Anatomy and Embryology, School of Basic Medical Sciences, Peking University Health Science Center, Beijing, China